

Metal adsorbate interactions and the convergence of density functional calculations

Christoph Rohmann,^{1,2} Maicol A. Ochoa,^{1,2} and Michael Zwolak^{1,*}

¹*Biophysics Group, Microsystems and Nanotechnology Division, Physical Measurement Laboratory, National Institute of Standards and Technology, Gaithersburg, MD 20899, USA*

²*Maryland NanoCenter, University of Maryland, College Park, Maryland 20783, USA*

(Dated: February 18, 2020)

The adsorption of metal atoms on nanostructures, such as graphene and nanotubes, plays an important role in catalysis, electronic doping, and tuning material properties. Quantum chemical calculations permit the investigation of this process to discover desirable interactions and obtain mechanistic insights into adsorbate behavior, of which the binding strength is a central quantity. Binding strengths, however, vary widely in the literature, even when using almost identical computational methods. To address this issue, we investigate the adsorption of a variety of metals onto graphene, carbon nanotubes, and boron nitride nanotubes. As is well-known, calculations on periodic structures require a sufficiently large system size to remove interactions between periodic images. Our results indicate that there are both direct and indirect mechanisms for this interaction, where the latter can require even larger system sizes than typically employed. The magnitude and distance of the effect depends on the electronic state of the substrate and the open- or closed-shell nature of the adsorbate. For instance, insulating substrates (e.g., boron nitride nanotubes) show essentially no dependence on system size, whereas metallic or semi-metallic systems can have a substantial effect due to the delocalized nature of the electronic states interacting with the adsorbate. We derive a scaling relation for the length dependence with a representative tight-binding model. These results demonstrate how to extrapolate the binding energies to the isolated-impurity limit.

Graphene, carbon nanotubes (CNTs), and boron nitride nanotubes (BNNTs) have exceptional mechanical, thermal, and electronic properties. These materials are thus the subject of intense research. Adsorption studies range from hydrogen and fluorine to metals of the 3d, 4d, and 5d series [1–18]. Among the latter are many density functional theory (DFT) studies examining the behavior of single metal atoms. These, however, show variation in the binding strengths up to several electron volts [5]. In part, this is due to differences in the methods employed, such as spin-polarized versus non-spin-polarized calculations, ultrasoft pseudo-potentials versus projector augmented wave methods (PAWs), or the use of LDA versus GGA exchange functionals. However, even studies employing almost identical techniques yield different results. For example, comparing the investigations of Manadé et al. [5], Pašti et al. [3] and Liu et al. [7] with respect to 3d metal adsorption, which all employed the same computational package, the Perdew–Burke–Ernzerhof Generalized-Gradient Approximation (PBE-GGA) exchange correlation functional, and PAWs, as well as a 4×4 graphene super cell, there are differences of up to 0.53 eV. From the information available, these studies differ in energy cut offs (450 eV to 600 eV), k -point meshes ($6 \times 6 \times 1$ to $10 \times 10 \times 1$), and the graphene layer spacings (1.5 nm to 2.0 nm). Although there are some differences in the approaches, the differences in binding energy are unexpectedly high given that DFT is regarded as well suited to study the effect of single atom adsorption.

Here, we investigate the binding energy dependence on the system size for various 3d metals on graphene, CNTs, and BNNTs by means of DFT. We aim to identify the cell size required to obtain, or extrapolate to, the isolated impurity limit, as well as understand related sources of error. Upon examining several metals on insulating, semi-conducting, semi-metallic, and conducting substrates, we observe a few classes of behavior. Some combinations of metals and substrates yield a slow decay or oscillatory behavior out to large system sizes. Other combinations show little-to-no cell-size dependence, as is consistently seen with metals on BNNTs. The use of different isolated atom calculations can also influence results, as can the size of the vacuum gap. By examining a one-dimensional tight-binding model, we demonstrate that the decay in binding strength, including decay of oscillations, behaves as the square of the inverse system size. The algebraic decay behaves as the square of the inverse rather than just the inverse due to periodicity. This scaling can be employed as a fitting form for more complex DFT calculations. These results provide insight into the adsorption behavior of metals on various substrates 1, as well as the errors incurred in common computational methods.

METHODOLOGY

We employ spin-polarized DFT calculations using the Vienna Ab initio Simulation Package (VASP) [19] and the PAW method [20] with the PBE-GGA functional. [21]. All structures are relaxed until the total energy converges to within 10^{-4} eV during the self-consistent loop, with forces converged to 0.1 eV/nm. An energy cut-off of 450 eV is used for all calculations. Van der Waals interactions are accounted for by the Grimme (D2) scheme [22]. The valence electron configuration for each metal considered are Al:2s²2p¹, Ti:3d³4s¹, Fe:3d⁷4s¹,

*Electronic address: mpz@nist.gov

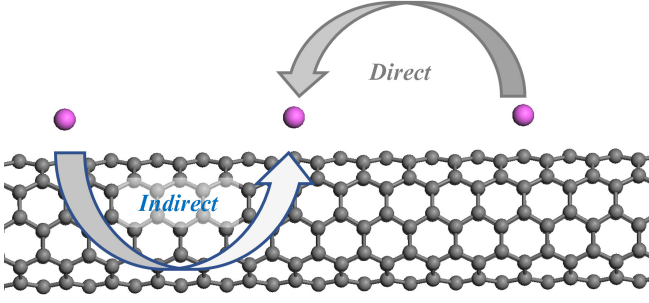


Figure 1: **Metal adsorption on a CNT.** Within DFT calculations, adsorbates “feel” their periodic images through both direct (via free space) and indirect (via the substrate) interactions. The latter can be substantial and have a long range.

V:3p⁶3d⁴4s¹, Ni:3d⁹4s¹, and Cu:3d¹⁰4s. The Methfessel-Paxton method with a smearing of 0.2 eV is taken for metal adsorption to metallic CNTs and graphene, whereas a Gaussian smearing of 0.02 eV is taken for semi-conducting CNTs and insulating BNNTs.

Prior to creating the supercells for the adsorption studies, the unit cell of each nanotube (NT) and the graphene sheet are optimized. The calculated parameters for the growth direction (c) of the nanotubes are 0.252 nm for the (5,5) BNNT, 0.247 nm for the (5,5) CNT, and 0.428 nm for the (8,0) CNT, respectively. In the case of graphene, the a and b lattice parameters are found to be 0.247 nm. In all models, a vacuum layer of at least 1.5 nm is added in a and b for the NTs and in c for graphene. To model the clean and adsorbate-covered structures, we examine nanotube system sizes up to 2.56 nm (for the (8,0) CNT adsorbing Al, system sizes go up to 3.84 nm while they are 3.42 nm in case of Ti and V), while the dimensions of the graphene system go up to 2.47 nm \times 2.47 nm. Table S1 (see supplementary material) lists the dimensions of nanotubes and graphene sheets in this work.

We perform extensive testing to obtain the required Monkhorst-Pack mesh [23] with the smallest cell for each system. In case of the (5,5) BNNT, this represents the $1 \times 1 \times 3$ supercell (0.741 nm) where a mesh of $1 \times 1 \times 2$ is found to be sufficient, while the $1 \times 1 \times 3$ supercell (0.755 nm) of the (5,5) CNT requires a $1 \times 1 \times 10$ mesh. In case of the (8,0) CNT, we employ a $1 \times 1 \times 2$ supercell (0.854 nm) where a k -point mesh of $1 \times 1 \times 5$ is required, with the exception of Al and V, which require a $1 \times 1 \times 7$ and $1 \times 1 \times 8$ mesh for convergence, respectively. Graphene in a 3×3 supercell (0.740 nm \times 0.740 nm) requires a mesh of $11 \times 11 \times 1$. The calculation precision (determined with these test systems) is maintained throughout our investigation, but the k -point mesh itself is not kept constant. For example, moving from a $1 \times 1 \times 3$ to a $1 \times 1 \times 6$ supercell in case of the (5,5) CNT allows us to employ a $1 \times 1 \times 5$ instead of a $1 \times 1 \times 10$ mesh while keeping the same precision. Details regarding the testing of the Monkhorst-Pack mesh and energy cut off are in the supplementary material, Tables S7-S11.

The binding energies, ΔE , for all systems are

$$\Delta E = E_S - E_X - E_M, \quad (1)$$

where E_S is the total energy of the simulated system, E_X is the energy of the adsorbate free substrate (graphene, CNT, or BNNT), and E_M is the energy of the isolated metal atom obtained at the gamma point in a cell identical or very close (in order to break symmetry) to the one used for E_S . Thus, for example, if E_S is obtained from a 3×3 graphene super cell, so is E_M .

We further employ a tight-binding (TB) Hamiltonian for a system consisting of a lattice of n atoms, which represents a model for the nanotube/graphene sheet, where each atom is a two-level system with degenerate orbitals. The energy of each atomic level is set to zero. The atomic orbitals of adjacent atoms overlap, introducing an electron hopping probability between them with coupling energy t . A single atom, represented by a single orbital, of zero energy ($\varepsilon_M = 0$), couples to the first atom with strength β . The resulting Hamiltonian \hat{H}_n is a $2n + 1$ square matrix of the form

$$\hat{H}_n = [0] \oplus (A_n \otimes T) + M_{2n+1}, \quad (2)$$

where T is the orbital coupling matrix

$$T = t \begin{bmatrix} 1 & 1 \\ 1 & 1 \end{bmatrix}, \quad (3)$$

A_n is the adjacency matrix with $\{i, j\}$ element

$$[A_n]_{i,j} = \delta_{i,j+1} + \delta_{i+1,j} + \delta_{1,i}\delta_{n,j} + \delta_{n,i}\delta_{1,j}, \quad (4)$$

and M_{2n+1} is the matrix for the metal-nanotube/graphene interaction

$$[M_{2n+1}]_{i,j} = \beta(\delta_{1,i}\delta_{j,2} + \delta_{1,i}\delta_{j,3} + \delta_{2,i}\delta_{j,1} + \delta_{3,i}\delta_{j,1}). \quad (5)$$

Molecular orbital energies ε_k are a result of diagonalizing \hat{H}_n . By setting $\beta = 0$, we recover the free systems (i.e., isolated impurities and pristine substrates). The binding energy is therefore the difference between the electronic energies of the bonded and unbonded system. Ordering the set of eigenenergies $\{\varepsilon_k\}$ such that $\varepsilon_k \leq \varepsilon_{k+1}$, the binding energy is $\sum_{k=1}^{n+1} \varepsilon_k(\beta) - \sum_{k=1}^{n+1} \varepsilon_k(\beta = 0)$, where the summation includes n electrons for the substrate (half-filling) plus one electron from the adatom [25].

RESULTS AND DISCUSSION

Adsorption Sites. We study the adsorption of Al, Ti, Fe, Ni, V, and Cu on graphene, CNTs, and BNNTs on several adsorption sites to determine the most stable configuration. In the case of graphene, these are the hollow (H), top (T), and bridge (B) sites, representing adsorption in the center of a 6-fold carbon ring, on top of a carbon, and between two carbon atoms, respectively. For adsorption on CNTs and BNNTs, we study the H site and two different B sites ($B1$ and $B2$, $BN1$ and $BN2$ in case of BNNTs). These represent bridge sites running parallel

to the growth direction ($B1 / BN1$) and a neighboring bridge site ($B2 / BN2$) at an angle of 60° to the former with respect to the (8,0) CNT. For the (5,5) CNTs (BNNTs) the $B1$ ($BN1$) site represents those running perpendicular to the growth direction of the NT with the $B2$ ($BN2$) site neighboring the former at an angle of 60° . Our calculations show that, irrespective of the system size, the preferred adsorption site remains the same. However, we do note small changes in the metal-carbon or metal-boron/nitrogen bond length upon an increase in system size. The adsorption sites are presented in Table S2 (in the supplementary material) and compare well with those of earlier investigations [3, 5, 16].

General Considerations. In the following, we show and discuss the changes in binding energy upon an increase in system size, as well as the effect of the isolated atom and inter-layer spacing (vacuum gap). In this regard, the energy of the free atom E_M , which might appear trivial, can have a significant impact on the binding strength. While using the identical cell size for the isolated atom and the adsorbed atom is a standard protocol, we examine its effect since it is often unclear whether this protocol is employed. In many calculations, the adsorbate, a single metal atom in our case, is simply placed in a $1 \text{ nm} \times 1 \text{ nm} \times 1 \text{ nm}$ cell, or a small variation of this to break the cubic symmetry. Not breaking the cubic symmetry of the cell can lead to an incorrect estimation of the ground state, as observed for Ni in our case. In our calculations, placing the metal atoms in the respective cells from the actual adsorption study leads to errors in the ground state of several tenths of an electron volt for Al, Ti, and V. In addition to this, one also needs to consider the lateral separation of adatoms in the E_X term in Eq. (1). Employing a 4×4 supercell of graphene (roughly, $1 \text{ nm} \times 1 \text{ nm}$) with a 1 nm and 2 nm vacuum layer separation yields a difference in energy of 0.4 eV for Fe adsorbing on the T site, whereas all other metals show a difference of less than 0.05 eV. This example illustrates the effect of the layer spacing on the binding energy. While adsorption at the T site results in a difference of 0.4 eV, the adsorption at the H site (which is still the most stable site) results in a difference of less than 0.05 eV when going from a 1 nm to a 2 nm layer spacing. The change in energy of the pure, adsorbate free graphene sheets is less than 0.03 eV in case of a 1 nm sheet separation, which is in agreement with earlier results [5].

However, to prevent the interaction with the periodic image, and to obtain a fully converged binding energy, one needs to consider the adsorbate covered system to determine the required cell size, since (i) the adsorbate by itself requires a certain cell size and (ii) the structural and electronic properties of the system will change due to the introduction of the adatom, which can also require the use of larger system cells. In some studies, a finite adsorbate coverage might be of interest. However, to study the adsorption of a single, isolated adsorbate, the system needs to be large enough to prevent the interaction of

periodic images, regardless of whether the added atom is adsorbed to the surface or free.

The effect of the free atom (essentially, direct interactions) is clearly seen in Fig. 2, which gives the binding energy versus the NT length or graphene sheet size. Here, the different systems are represented by different colors, whereas the binding energy is shown as squares and triangles. The squares represent the binding energy from the absolute ground state of the free atom (the free atom in a cell large enough to prevent interactions with its periodic image) and the triangles represent results from the free atom in the respective adsorption cell. The latter is at times very small and thus results in significant interactions of the atom with its periodic image. In case of graphene, this is a stronger effect due to the fact that it is a 2D material, while the NTs are 1D. Thus, the periodic image is ‘felt’ from the x and y direction in graphene while only in the z direction in case of the NTs, since one can extend the vacuum gap in the other directions. To provide an additional perspective on these findings, we include a substrate-based version of Fig. 2 in the supplementary material (Fig. S4).

System Size and Metal Type. Examining the trend of binding energy versus system size, Fig. 2, we note the following: (i) that insulating systems are least affected by the system size, whereas metallic systems – the (5,5) CNT and graphene, which is turned into a metallic system after metal atom adsorption – exhibit the largest changes in ΔE . (ii) We do not achieve full convergence – convergence to within the estimated DFT error of 0.01 eV [26] – of the binding energy for Ti, V, and Fe adsorbing to metallic substrates for system sizes with linear dimension of greater than 2.4 nm. (iii) For adsorption on the semiconducting (8,0) CNT, there is a marginal but steady increase in the binding energy for Al and a decrease for Ti and V up to roughly 2.7 nm. Further increasing the length of the system shows that Al, Ti and V are actually converged at a 2.7 nm length of the (8,0) CNT (not shown in Fig. 2). The observations (i) and (ii), together with the fact that free atom calculations are fully converged for the larger cells (see the overlap of square and triangle data points), indicates that there is a quasi-long range interaction between metal adsorbates and their periodic images. This interaction that proceeds through the substrate is strongest through metallic substrates. We can thus distinguish between direct – i.e., through free space – and indirect – i.e., through the substrate – mechanisms for adsorbate-adsorbate interactions 1.

We note that Cu is an exception to observation (i), with a binding energy that changes only as the system size increases from $\approx 0.8 \text{ nm}$ to $\approx 1 \text{ nm}$ for the (5,5) CNT and graphene. A possible explanation could stem from the fact that Cu is the only d^{10} metal in our study and has, together with Ni, the highest electronegativity among the metals we examine. Considering Ni in this respect, it is not surprising that it shows only small changes in ΔE for the metallic systems. Ni is a d^9 metal,

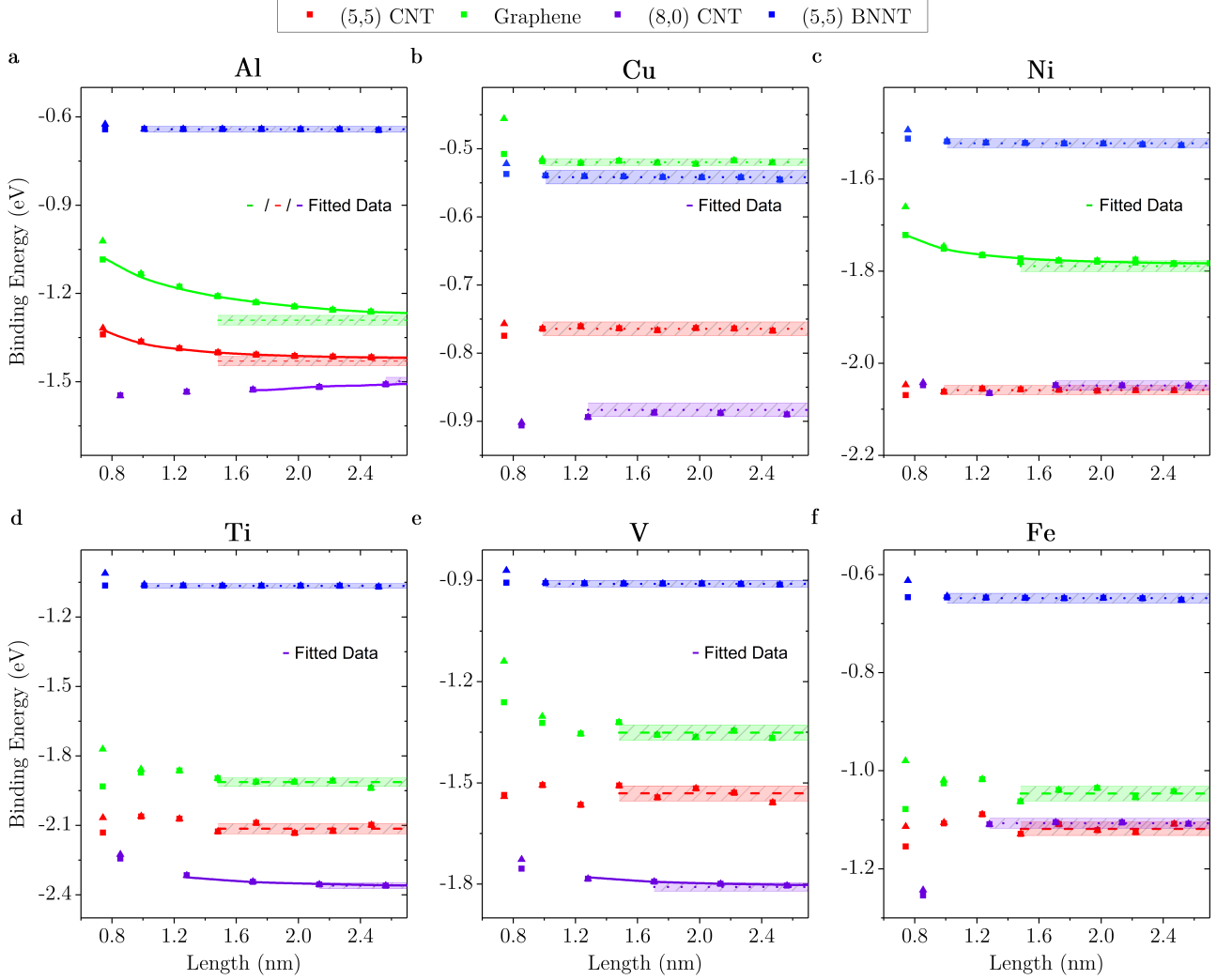


Figure 2: **Binding energies versus system size.** Here, the blue, purple, green, and red data points represent the insulating (5,5) BNNT, semiconducting (8,0) CNT, zero-point semiconductor graphene, and the metallic (5,5) CNT, respectively. The squares show the results using the absolute ground state energy of the free atoms, whereas the triangles represent the results from the free atom in the respective adsorption size cells. A dotted line indicates fully converged DFT data, whereas dashed lines indicate the extrapolated binding energy (numerical fitting to Eq. 8 in case of Al for the (5,5) CNT and graphene) or averaged binding energy over the indicated data points (V, Fe, and Ti for graphene and the (5,5) CNT). In all cases, the shaded area represents the error in the binding energy originating from the DFT calculations. The solid line represents a fit to the scaling form in Eq. (8) from the TB model. In the determination of the fitting parameters, only data points for the longer NT system sizes and larger graphene sheets are considered since Eq. (8) is the asymptotic expression for the binding energy, see supplementary material. We estimate the error variance $\delta E = \pm \sqrt{\sigma_{DFT}^2 + \sigma_{\Delta E_\infty}^2}$ using the fitting error $\sigma_{\Delta E_\infty}$ (Table S6 in the see supplementary material for more information). The estimated error in the DFT calculations $\sigma_{DFT} = 0.01$ eV. In cases that use an average value for the binding energy, the error represents the maximal difference in energy of the data points considered for averaging.

unlike Cu. However, upon adsorption Ni's 4s electron is filling the d-orbitals, while a small portion of its electron density is donated to graphene due to the higher electronegativity of C compared to Ni. Ni's d-orbitals are thus close to, but less than, full occupancy. One can therefore assume a similar behavior with Cu. Indeed, Ni

and Cu show an almost identical behavior for adsorption to the insulating (5,5) BNNT and semiconducting (8,0) CNT, and are essentially converged above about 1.5 nm for the metallic systems.

In contrast, Fe, Ti, and V, see Fig. 2d-f, show larger, although still small, fluctuations in binding energy even

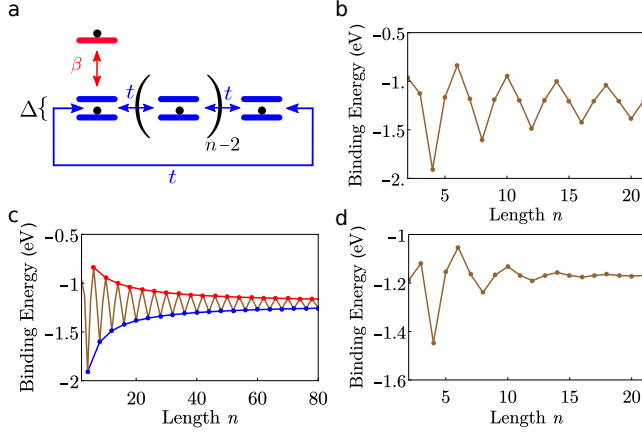


Figure 3: **Tight-binding model for metal-nanotube/graphene binding energies.** (a) A model one-dimensional substrate consisting of a periodic lattice of n two-level atoms, a nearest neighbor interaction t , and adsorbate-substrate interaction β to the first atom in the system only. (b) Binding energies versus the system length n when the energy gap is zero, $\beta = 1.2$ eV, and $t = 1.25$ eV. (c) Binding energies for the same parameters as in (b) but for the system length taking only values $n = 4k + 6$ (red) and $n = 4k + 4$ (blue) with k an integer. (d) Binding energies versus n with an energy gap Δ between the two levels of 0.4 eV (but otherwise the parameters are the same as in (b)), thus giving a representation of an insulating or semiconducting system n .

at the largest system sizes for the metallic systems. Further increasing the cell dimension to 3 nm, reducing the k -point spacing by a factor of three, employing a gamma point centered grid or eliminating the small aliasing errors in VASP calculations (via sufficiently high settings) all fail to reduce or eliminate these fluctuations and trends. It is likely that these fluctuations represent physical, Friedel-like oscillations, as they appear upon binding to metals and semiconductors. Ti, Fe, and V all have an open 3d shell, whereas Cu and adsorbed Ni are d^{10} and nearly d^{10} , respectively, which may be the underlying cause of their different behavior.

We further note the existence of many local minima close to the identified global minimum for large cells of graphene with the adsorption of Cu, Ni, and Fe. In order to identify the most stable adsorption site, a variety of different geometries were tested around where we believe the global minima is situated. This could cause oscillations in binding energies as well. However, upon extensive testing, it seems unlikely to be responsible for the oscillations seen for Fe, but it may be causing the minute deviation of the last data points for Ni and Cu in case of graphene and the (5,5) CNT respectively.

To investigate these fluctuations further, we examine the use of D3 (Grimme) calculations on metal adsorption to the (5,5) CNT. Although the absolute binding energies are different, the overall trend and fluctuations remain the same, see Fig. S6 in the supplementary material for

more details.

Next, we examine the tight-binding model of Fig. 3a. This particular model has no direct adsorbate-adsorbate interaction and thus allows us to examine solely the effect of indirect interactions. The size of the system is proportional to the number n of atoms in the system. Figure 3b,c shows that the binding energies converge for large system sizes, following an oscillatory pattern. Convergence is faster when there is an energy gap, as seen in Fig. 3d, where it is also seen that the oscillations are more effectively damped. The latter behavior is qualitatively similar to much of the oscillatory behavior seen in the DFT calculations. Moreover, how the system size is increased can lead to a monotonic increase ($n = 4k + 4$ with k an integer) or decrease ($n = 4k + 6$) towards the asymptotic (isolated impurity) limit. Thus, the range of behavior given by DFT indicates intrinsic, physical behavior and not something particular to the method of calculation.

For the tight-binding model in Fig. 3a, we can provide an analytic estimate for the convergence with the cell length. From the exact energy eigenvalues and eigenstates for the unbound system and taking the coupling strength β as the perturbation parameter, the binding energy versus n is

$$\Delta E = \left(\frac{\beta^2}{t} - \frac{\beta^4}{8t^3} \right) \times I_n, \quad (6)$$

up to 4th order in β . In Eq. (6), the term I_n carries the length dependence and is explicitly given by

$$I_n = \frac{1}{n} \sum_{k \geq n/4}^{3n/4} \cos(2\pi k/n), \quad (7)$$

where we use the fact that the Fermi level is at half filling [27]. The quantity I_n has the form of a Riemann sum, and converges to $-1/\pi$, as n goes to infinity. As a result, ΔE reaches the asymptotic value as some power of $1/n$ [24]. Since the linear dimension L of the system is proportional to n , the binding energy ΔE decays as

$$\Delta E(L) = \Delta E(\infty) + \frac{B}{L^2}, \quad L \rightarrow \infty, \quad (8)$$

where B is a coefficient that depends on the specific function in the Riemann sum (for more details see the supplemental material). This coefficient can be both positive or negative (see Fig. 3c) and can also oscillate (but remain bounded so that the asymptotic decay is $1/L^2$ but oscillatory). We emphasize that Eq. (8) describes the asymptotic decay to the limit binding energy $\Delta E(\infty)$ and the exact dependence on L for smaller cells might be different.

This decay and other tight-binding results are in qualitative agreement with the DFT results. Both show that (i) a larger sheet or longer NT is required to obtain a converged binding energy in case of a metallic system, see the respective graphene and (5,5) CNT (green and

red data points, respectively) systems of Al, Cu, and Ni in Fig. 2 a-c in comparison to Fig. 3c. (ii) Systems with a band gap converge faster than their metallic counterparts, see the (8,0) CNT (purple data points) and (5,5) BNNT (blue data points) semiconducting and insulating systems versus the metallic graphene and (5,5) CNT systems (green and red data points, respectively) in Fig. 2 in comparison to Fig. 3b versus 3d. (iii) The tight-binding model shows fluctuations in the binding energy for metallic systems, see Fig. 3b and c, even at a larger system size which we also note in case of graphene and the (5,5) CNT for the open shell systems of Fe, Ti, and V, see Fig. 2d-f. Thus, we provide evidence that the fluctuation noted for Ti, V, and Fe are real and do not stem from particular choices of DFT parameters or methods.

In addition, the decay form, Eq. (8), gives a method to scale finite-size results and extrapolate to the isolated impurity limit. For example, Fig. 2 a shows Eq. (8) fit to the binding energy decay for Al on the (5,5) CNT and graphene (solid red and green lines respectively), along with the value of $\Delta E(\infty)$ and error bars from the respective DFT calculations. In principle, it is possible to employ Eq. (8) for all DFT results, including the oscillatory behavior. However, the accessible range of length scales due to computational resources and the estimated error in DFT make fitting oscillatory B error-prone. There are not enough data points, and even if there were, the decay would put the value at finite L to within the error of our DFT calculations (0.01 eV). We thus separate the DFT results into three classes, ones with monotonic decay (Al on the (5,5) CNT, graphene, and the (8,0) CNT, as well as Ti and V on the (8,0) CNT), ones with rapid convergence [Cu and Ni; and all metals on BNNTs], and those with oscillatory behavior (Ti, V, and Fe on the (5,5) CNTs and graphene). The first two classes can make use of the scaling form, although the second class does not need it since the result is effectively $\Delta E(\infty)$, except for the smallest cell sizes considered. Error bars for the cases are defined in terms of the fit errors. For the third class, we propose a heuristic method: take a range of the largest cell sizes accessible (in our case, cells from 1 nm or 1.5 nm to 2.7 nm), compute the average ΔE within that range,

which averages over some of the oscillations, and use the standard deviation to quantify the error. The isolated impurity binding energies for all metals and systems is shown in Table S3 (see supplementary material).

CONCLUSION

Our results yield the magnitude of direct and indirect interactions for metal atom adsorption on common substrates (graphene and metallic, semiconducting, and insulating NTs). The factors that influence the strength of these interactions and/or the computed binding strengths are (i) the nature of the substrate (metallic, semiconducting or insulating), (ii) the closed or open shell structure of the metal, (iii) the method of computing the isolated atom energies, and (iv) the size of the simulation cell (both in the direction(s) of the substrate and any vacuum gap between structures). Insulating systems generally require the smallest simulation sizes followed by semi-conducting and metallic systems. Open shell systems, such as Fe, V, and Ti, do not fully converge, but rather show a fluctuating – but decaying – binding energy at larger simulation cell sizes. We derive a scaling relation that permits the extrapolation of smaller simulation cell results out to the infinite simulation cell limit (i.e., a fully isolated impurity). This enables a more effective calculation of binding in slowly converging systems, such as Al on graphene and the (5,5) CNT. Overall, this scaling relation and a simple heuristic for oscillatory systems yields a framework for determining binding energies and providing error estimates.

SUPPLEMENTARY MATERIAL

See supplementary material for the convergence tests, the D3 versus D2 results, a detailed derivation of Eq. (8), the binding energies from 1D-tight binding models, and the criteria for the numerical fittings.

ACKNOWLEDGMENTS

We thank J. Elenewski and S. Sahu for helpful discussions. C. R. and M. A. O. acknowledge the support under the Cooperative Research Agreement between the University of Maryland and the National Institute of Standards and Technology Physical Measurements Laboratory, Award 70NANB14H209, through the University of Maryland.

-
- [1] A. J. M. Giesbers, K. Uhlířová, M. Konečný, E. C. Peters, M. Burghard, J. Aarts, and C. F. J. Flipse, *Phys. Rev. Lett.* **111**, 166101 (2013).
 - [2] X. Hong, K. Zou, B. Wang, S.-H. Cheng, and J. Zhu, *Phys. Rev. Lett.* **108**, 226602 (2012).
 - [3] I. A. Pašti, A. Jovanović, A. S. Dobrota, S. V. Mentus, B. Johansson, and N. V. Skorodumova, *Appl. Surf. Sci.* **436**, 433 (2018).
 - [4] N. Dimakis, F. A. Flor, A. Salgado, K. Adjibi, S. Vargas, and J. Saenz, *Appl. Surf. Sci.* **421**, 252 (2017).
 - [5] M. Manadé, F. Viñes, and F. Illas, *Carbon* **95**, 525 (2015).
 - [6] B. F. Habenicht, D. Teng, L. Semidey-Flecha, D. S. Sholl, and Y. Xu, *Top. Catal.* **57**, 69 (2014).
 - [7] X. Liu, C. Z. Wang, M. Hupalo, W. C. Lu, M. C. Tringides, Y. X. Yao, and K. M. Ho, *Phys. Chem. Chem. Phys.* **14**, 9157 (2012).
 - [8] H. Zhang, C. Lazo, S. Blügel, S. Heinze, and Y. Mokrousov, *Phys. Rev. Lett.* **108**, 056802 (2012).
 - [9] K. Nakada and A. Ishii, *Solid State Commun.* **151**, 13 (2011).
 - [10] H. Valencia, A. Gil, and G. Frapper, *J. Phys. Chem. C* **114**, 14141 (2010).
 - [11] M. Sargolzaei and F. Gudarzi, *J. Appl. Phys.* **110**, 064303 (2011).
 - [12] J. Ding, Z. Qiao, W. Feng, Y. Yao, and Q. Niu, *Phys. Rev. B* **84**, 195444 (2011).
 - [13] E. J. G. Santos, D. Sánchez-Portal, and A. Ayuela, *Phys.*

- Rev. B **81**, 125433 (2010).
- [14] V. Zólyomi, Á. Ruzsnyák, J. Kürti, and C. J. Lambert, J. Phys. Chem. C **114**, 18548 (2010).
 - [15] L. Hu, X. Hu, X. Wu, C. Du, Y. Dai, and J. Deng, Physica B **405**, 3337 (2010).
 - [16] C. Rohmann, Q. Sun, and D. J. Searles, J. Phys. Chem. C **120**, 3509 (2016).
 - [17] J.-M. Zhang, S.-F. Wang, L.-Y. Chen, K.-W. Xu, and V. Ji, Eur. Phys. J. B **76**, 289 (2010).
 - [18] C. Rohmann, V. I. Yamakov, C. Park, C. Fay, M. Hankel, and D. J. Searles, J. Phys. Chem. C (2018).
 - [19] G. Kresse and J. Furthmüller, Phys. Rev. B **54**, 11169 (1996).
 - [20] G. Kresse and D. Joubert, Phys. Rev. B **59**, 1758 (1999).
 - [21] J. P. Perdew, K. Burke, and M. Ernzerhof, Phys. Rev. Lett. **77**, 3865 (1996).
 - [22] S. Grimme, J. Comput. Chem. **27**, 1787 (2006).
 - [23] H. J. Monkhorst and J. D. Pack, Phys. Rev. B **13**, 5188 (1976).
 - [24] C. K. Chui, J. Approx. Theory **4**, 279 (1971).
 - [25] Disclaimer: Certain commercial products are identified in this paper in order to specify the theoretical procedure adequately. Such identification is not intended to imply recommendation or endorsement by the National Institute of Standards and Technology nor is it intended to imply that the software identified is necessarily the best available for the type of work.
 - [26] We estimate the error in our DFT calculations by conducting multiple test calculations with Al adsorbing to graphene. A variety of different initial positions for Al are tested. The error results from the largest difference in binding strength of all structures where Al is found at the *H* site (the preferred adsorptions site) after optimization. The largest difference is noted as 0.006 eV. Therefore we estimate an error of 0.01 eV for all metals and systems investigated.
 - [27] Note that the summation index *k* takes integer values between $\frac{n}{4}$ and $\frac{3n}{4}$.

Supplementary Material – Metal adsorbate interactions and the convergence of density functional calculations

Christoph Rohmann,^{1,2} Maicol A. Ochoa,^{1,2} and Michael Zwolak¹

¹*Biophysics Group, Microsystems and Nanotechnology Division, Physical Measurement Laboratory, National Institute of Standards and Technology, Gaithersburg, MD 20899, USA*

²*Maryland NanoCenter, University of Maryland, College Park, Maryland 20783, United States*

(Dated: February 18, 2020)

I. SINGLE-ATOM BINDING

CNT	Length in c (nm)							
(8,0)	0.854	1.281	1.708	2.135	2.562			
(5,5)	0.741	0.988	1.235	1.482	1.729	1.976	2.223	2.470
BNNT	Length in c (nm)							
(5,5)	0.755	1.007	1.259	1.511	1.763	2.014	2.266	2.518
Graphene	Dimensions in a and b (nm)							
	0.740	0.987	1.234	1.481	1.728	1.974	2.221	2.468

Table S1: **Cell parameters.** The dimensions of the super cells in direction c for the different nanotube lengths, as well as in a and b for the width and length of the graphene sheet.

Metal/Systems	Al	Ti	V	Fe	Ni	Cu
Graphene	H	H	H	H	H	T
(5,5) CNT	H	H	H	H	T	B
(8,0) CNT	H	H	H	H	B	B
(5,5) BNNT	$BN1$	H	T	$BN1$	T	$BN1$

Table S2: **Adsorption sites.** The preferred adsorption sites of the metals on the respective NTs and graphene with H , T , and B indicating the adsorption to the hollow, top, and bridge sites, respectively. The $BN1$ site represents a bridging position between N and B running perpendicular to the growth direction of the BNNT. The T site adsorption in the case of Ni and V adsorbing on the (5,5) BNNTs takes place above a N atom. For each system, three different adsorption sites were tested. In each case, the preferred adsorption site remained the same regardless of system size. For example, although the H , T , and B are always tested, the H site was found to be the most stable adsorption site for Al adsorbing on graphene regardless of the system size.

ΔE (eV)	Al	Ti	V
Graphene	-1.29 ± 0.016	-1.91 ± 0.018	-1.35 ± 0.023
(5,5) CNT	-1.43 ± 0.016	-2.11 ± 0.022	-1.53 ± 0.022
(8,0) CNT	-1.51 ± 0.013	-2.38 ± 0.013	-1.79 ± 0.012
(5,5) BNNT	-0.64 ± 0.010	-1.07 ± 0.010	-0.91 ± 0.010
ΔE (eV)	Fe	Ni	Cu
Graphene	-1.05 ± 0.015	-1.78 ± 0.012	-0.52 ± 0.010
(5,5) CNT	-1.12 ± 0.013	-2.06 ± 0.010	-0.76 ± 0.010
(8,0) CNT	-1.11 ± 0.010	-2.05 ± 0.010	-0.89 ± 0.010
(5,5) BNNT	-0.91 ± 0.010	-1.52 ± 0.010	-0.54 ± 0.010

Table S3: **Binding Energies.** $\Delta E_X(\infty)$ for $X = \text{Al, Ti, V, Fe, Ni, and Cu}$ on different substrates (Graphene, CNT, BNNT). These values are obtained from fully converged DFT calculations by either fitting the data to the form in Eq. (8), or by averaging over the energies for the largest systems employed. See Fig. 2 and the main text for the error calculation method and additional details.

II. 1D-TIGHT BINDING MODEL

In this section, we calculate the binding energy for the tight-binding model in Fig. 3, reported within the main text in Eq. (6). In summary, starting from the eigenvalues and eigenvectors for the periodic 1D-lattice, we calculate the energy for metal-nanotube system utilizing perturbation theory, where the metal-nanotube coupling strength β is taken as the perturbation parameter.

First, we consider a simple model consisting of n single levels, tunneling constant t , and Hamiltonian

$$[\hat{H}_n]_{i,j} = t(\delta_{i,j+1} + \delta_{i+1,j} + \delta_{i,1}\delta_{j,n} + \delta_{i,n}\delta_{j,1}). \quad (\text{S1})$$

The system is periodic and consequently the Hamiltonian is invariant under discrete space translations. This also implies that each eigenvector $|\alpha_l\rangle$ – that we find by solving the eigenvalue equation $\hat{H}_n|\alpha_l\rangle = \alpha_l|\alpha_l\rangle$ for $l = 1, \dots, n$ – is periodic. Thus, the unnormalized complex eigenvector is

$$|\alpha_l\rangle = (e^{i\frac{2\pi}{n}l}, e^{i\frac{4\pi}{n}l}, \dots, e^{i\frac{2\pi k}{n}l}, \dots, e^{i\frac{2\pi(n-1)}{n}l}, 1)^T, \quad (\text{S2})$$

and from the eigenvalue equation we obtain the relation

$$te^{i\frac{2\pi(k-1)}{n}l} - \alpha_l e^{i\frac{2\pi k}{n}l} + te^{i\frac{2\pi(k+1)}{n}l} = 0 \quad (\text{S3})$$

from which we find the l eigenenergy α_l

$$\alpha_l = 2t \cos\left(\frac{2\pi l}{n}\right). \quad (\text{S4})$$

We notice that the complex conjugate of $|\alpha_l\rangle$ is also an eigenvector with eigenvalue α_l , and consequently $(1/2)(|\alpha_l\rangle + |\alpha_l\rangle^*)$ is the real eigenvector. The normalized real l eigenvector is

$$|\alpha_l\rangle = \sqrt{\frac{2}{n}} \left(\cos\left(\frac{2\pi}{n}l\right), \dots, \cos\left(\frac{2\pi k}{n}l\right), \dots, 1 \right)^T. \quad (\text{S5})$$

Finally, the energy for this system, with electron density n_e/n , is the sum of the lowest n_e eigenvalues.

Next, we consider that an atom, represented by a single energy level of zero energy, binds to the first site in the periodic lattice, with coupling strength β . The Hamiltonian for the composite system is

$$\hat{H} = [0] \oplus \hat{H}_n + \beta \hat{V}, \quad (\text{S6})$$

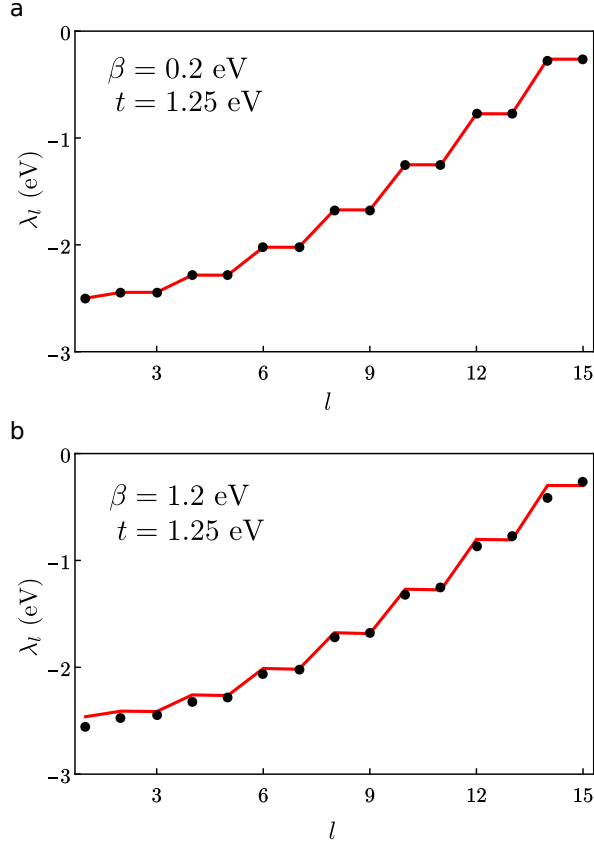


Figure S1: **Exact and approximate eigenvalues of the tight-binding model.** Comparison between the exact (dots, black) and approximate lowest eigenvalues (solid, red) for the 1D tight-binding model and unit size cell $n = 30$. Here λ_l is the eigenvalue for state l .

where \hat{V} is an $(n + 1)$ -dimensional square matrix with entries $[\hat{V}]_{i,j} = \delta_{i,1}\delta_{j,2} + \delta_{i,2}\delta_{j,1}$. Taking β as the perturbation parameter, the eigenvectors basis for the unperturbed system consists of

$$|\lambda_0^{(0)}\rangle = (1, 0, \dots, 0) \quad (\text{S7})$$

$$|\lambda_l^{(0)}\rangle = (0) \oplus |\alpha_l\rangle \quad (1 \leq l \leq n), \quad (\text{S8})$$

with zeroth order eigenenergies $\lambda_0^{(0)} = 0$ and $\lambda_l^{(0)} = \alpha_l$. We can write the eigenenergies λ_l for the composite system up to second order

$$\lambda_l^{(2)}(\beta) = \lambda_l^{(0)} + \beta \langle \lambda_l^{(0)} | \hat{V} | \lambda_l^{(0)} \rangle + \beta^2 \sum_{r \neq l} \frac{|\langle \lambda_l^{(0)} | \hat{V} | \lambda_r^{(0)} \rangle|^2}{\lambda_l^{(0)} - \lambda_r^{(0)}}, \quad (\text{S9})$$

which is further simplified by noticing that

$$\langle \lambda_l^{(0)} | \hat{V} | \lambda_l^{(0)} \rangle = 0 \quad (\text{S10})$$

$$\langle \lambda_r^{(0)} | \hat{V} | \lambda_l^{(0)} \rangle = 0 \quad (r, l \geq 1) \quad (\text{S11})$$

$$\langle \lambda_0^{(0)} | \hat{V} | \lambda_l^{(0)} \rangle = \sqrt{\frac{2}{n}} \cos\left(\frac{2\pi}{n}l\right) \quad (l \geq 1). \quad (\text{S12})$$

Therefore

$$\lambda_0^{(2)}(\beta) = \lambda_0^{(0)} = 0, \quad (\text{S13})$$

$$\lambda_l^{(2)}(\beta) = \lambda_l^{(0)} + \frac{\beta^2}{nt} \cos\left(\frac{2\pi}{n}l\right) \quad (l \geq 1). \quad (\text{S14})$$

If $n = 2n_e$, then the binding energy up to second order is

$$\Delta E_n^{(2)} = \sum_{l < \text{LUMO}} \lambda_l^{(2)}(\beta) - \lambda_l^{(0)} \quad (\text{S15})$$

$$= \frac{\beta^2}{nt} \sum_{l \geq n/4}^{l \leq 3n/4} \cos\left(\frac{2\pi}{n}l\right) \quad (\text{S16})$$

The present analysis can be extended to include higher order corrections in the perturbation expansion. Since several matrix elements in the perturbation Hamiltonian cancel, Eqs. (S10)-(S12), we can carry out the full summation over higher order terms in the perturbation. For example, the forth order form of the binding energy is

$$\Delta E_n^{(4)} = \left(\frac{\beta^2}{t} - \frac{\beta^4}{2t^3} \right) I_n, \quad (\text{S17})$$

where I_n is defined in Eq. (6).

These results can be extended to the model in Fig. 3, where each site has two degenerate levels ($\Delta = 0$). For this, notice that the tunneling matrix T in Eq. (3) is singular, and therefore the rank of the Hamiltonian \hat{H}_n in Eq. (2) for $\beta = 0$ is n . As a result, the system has n zero eigenenergies and, after performing elementary operations, a submatrix of size n of the form in Eq. (S1) is recovered with t replaced by $2t$.

Returning to the second order expression for the binding energy, the limit value, $\Delta E^{(2)} = \lim_{n \rightarrow \infty} \Delta E_n^{(2)}$, is the real binding energy for a single atom. We calculate this limit as

$$I = \lim_{n \rightarrow \infty} I_n = \lim_{n \rightarrow \infty} \frac{1}{n} \sum_{l \geq n/4}^{l \leq 3n/4} \cos\left(\frac{2\pi}{n}l\right) \quad (\text{S18})$$

$$= \frac{1}{2\pi} \lim_{n \rightarrow \infty} \sum_{l \geq n/4}^{l \leq 3n/4} \frac{2\pi}{n} \cos\left(\frac{2\pi}{n}l\right) \quad (\text{S19})$$

Next, we let $\theta_l = (2\pi/n)l$ and $\Delta\theta = \theta_{l+1} - \theta_l = (2\pi/n)$,

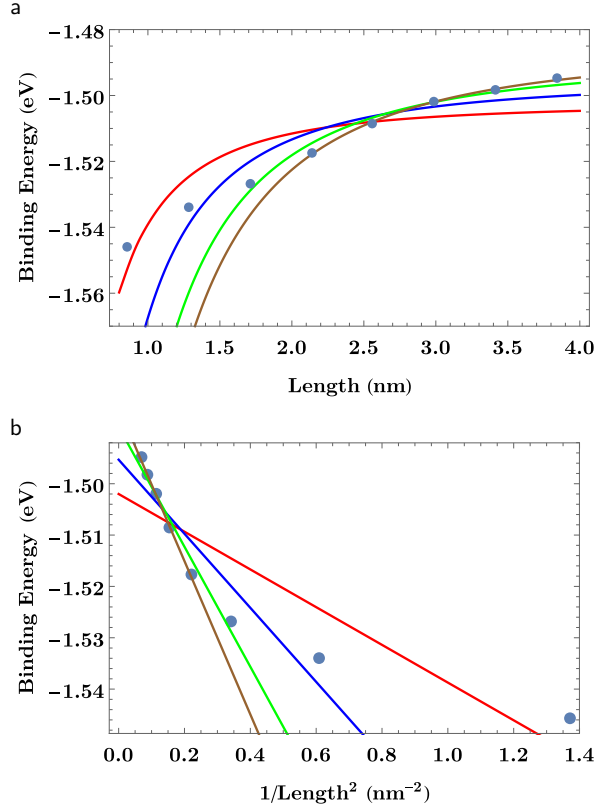


Figure S2: **Binding Energy Dependence Al/(8,0) CNT.** DFT Binding energies for Al in CNT (8,0) as a function of (a) unit cell size and (b) the inverse squared unit cell size. We include fitting curves Eq. (8) for several fitting parameters B and $\Delta E(\infty)$ obtained from the last m points: (red) $m = 8$, (blue) $m = 7$, (green) $m = 6$, and (brown) $m = 5$. The value for the fitting parameters are in reported in Table S4.

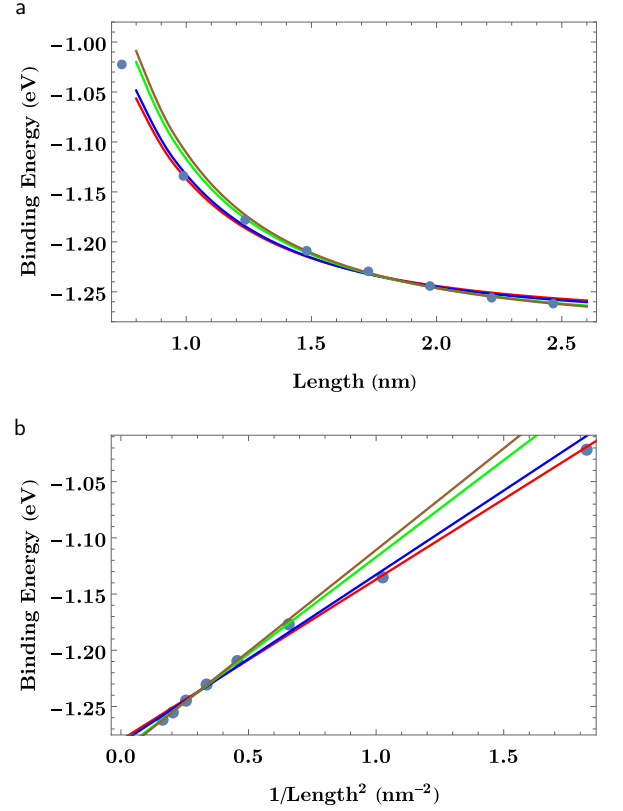


Figure S3: **Binding Energy Dependence Al/Graphene.** DFT Binding energies for Al in Graphene as a function of (a) unit cell size and (b) the inverse squared unit cell size. We include fitting curves Eq. (8) for several fitting parameters B and $\Delta E(\infty)$ obtained from the last m points: (red) $m = 8$, (blue) $m = 7$, (green) $m = 6$, and (brown) $m = 5$. The value for the fitting parameters are in reported in Table S5.

such that

$$I = \frac{1}{2\pi} \lim_{n \rightarrow \infty} \sum_{\theta_l \geq \pi/2}^{3\pi/2} \Delta\theta \cos(\theta_l) \quad (\text{S20})$$

$$= \frac{1}{2\pi} \int_{\pi/2}^{3\pi/2} d\theta \cos(\theta) = -\frac{1}{\pi}. \quad (\text{S21})$$

Therefore,

$$\Delta E^{(2)} = -\frac{\beta^2}{t\pi}. \quad (\text{S22})$$

An alternative form for I that we use in the next section, resulting from the change of variables $y = (2/\pi)\theta$ is

$$I = \frac{1}{4} \int_1^3 dy \cos\left(\frac{\pi y}{2}\right). \quad (\text{S23})$$

III. ASYMPTOTIC DECAY

In this section we show that for the tight-binding model, binding energies converge to their asymptotic

value as the inverse of the square of the length of the unit cell ($1/n^2$). This result motivates the fitting function Eq. (8). The Riemman sum in Eq. (S21) can be written as an integral, after introducing the floor function $\lfloor x \rfloor$. First we note that

$$\Delta\theta \cos(\Delta\theta l) = \frac{2\pi}{n} \int_l^{l+1} dx \cos\left(\frac{2\pi}{n} \lfloor x \rfloor\right) \quad (\text{S24})$$

$$= \frac{\pi}{2} \int_{4l/n}^{4(l+1)/n} dy \cos\left(\frac{2\pi}{n} \left\lfloor \frac{ny}{4} \right\rfloor\right) \quad (\text{S25})$$

Therefore

$$I_n = \frac{1}{4} \int_1^{3+4/n} dy \cos\left(\frac{2\pi}{n} \left\lfloor \frac{ny}{4} \right\rfloor\right) \quad (\text{S26})$$

and

$$I_n - I = \frac{1}{4} \int_1^3 dy \left[\cos\left(\frac{2\pi}{n} \left\lfloor \frac{ny}{4} \right\rfloor\right) - \cos\left(\frac{2\pi ny}{4}\right) \right] + \frac{1}{4} \int_3^{3+4/n} dy \cos\left(\frac{2\pi}{n} \left\lfloor \frac{ny}{4} \right\rfloor\right). \quad (\text{S27})$$

For $n = 4m$, the integrand in the second term in Eq. (S27) equals $\cos(3\pi/2) = 0$. Next, we write $\cos\left(\frac{2\pi}{n} \frac{ny}{4}\right)$ as a Taylor expansion up to second order around the integer $\lfloor \frac{ny}{4} \rfloor$

$$\begin{aligned} \cos\left(\frac{2\pi}{n} \frac{ny}{4}\right) &= \cos\left(\frac{2\pi}{n} \left\lfloor \frac{ny}{4} \right\rfloor\right) \\ &\quad - \left(\frac{ny}{4} - \left\lfloor \frac{ny}{4} \right\rfloor\right) \left(\frac{2\pi}{n}\right) \sin\left(\frac{2\pi}{n} \left\lfloor \frac{ny}{4} \right\rfloor\right) \\ &\quad + \frac{1}{2} \left(\frac{ny}{4} - \left\lfloor \frac{ny}{4} \right\rfloor\right)^2 \left(\frac{2\pi}{n}\right)^2 \cos\left(\frac{2\pi}{n} \left\lfloor \frac{ny}{4} \right\rfloor\right) \end{aligned} \quad (\text{S28})$$

and substitute into Eq. (S27). We notice that $\sin\left(\frac{2\pi}{n} \left\lfloor \frac{ny}{4} \right\rfloor\right)$ converges to the function $\sin\left(\frac{2\pi}{n} \frac{ny}{4}\right)$, which is an odd function with respect to $y = 2$ and therefore

$$\int_1^3 \sin\left(\frac{2\pi}{n} \left\lfloor \frac{ny}{4} \right\rfloor\right) dy \rightarrow 0, \quad (\text{S29})$$

as $O(1/n)$. Consequently

$$I_n - I = -\frac{\pi^2}{2n^2} \int_1^3 dy \left(\frac{ny}{4} - \left\lfloor \frac{ny}{4} \right\rfloor\right) \cos\left(\frac{2\pi}{n} \left\lfloor \frac{ny}{4} \right\rfloor\right) \quad (\text{S30})$$

which implies that

$$|I_n - I| \leq \frac{\pi^2}{n^2}. \quad (\text{S31})$$

IV. NUMERICAL FITTINGS

In this section, we illustrate how the DFT binding energies are fitted to Eq. (8) in the main text, and consequently how we obtain $\Delta E(\infty)$ in the case of binding energies that monotonically converge as a function of unit cell size. We consider Al in (8,0) CNT in Fig. S2 and Table S4, and Al in graphene in Fig. S3 and Table S5 as representative examples. The result in Eq. (8) is a good representation of the functional form of the binding energy for unit cell sizes that are large. This observation is confirmed in Figs. S2 and S3, where we present several fitting curves obtained by sequentially disregarding the binding energies from smaller unit cells. Indeed, the asymptotic relation Eq. (8) has a coefficient of determination, r^2 , to the DFT binding energies bigger than 0.99 for the fitting that considers only unit-cell sizes bigger than 2 nm. We utilize this criteria in several systems and report the obtained fitting parameters in Table S6. We also present in Fig. S4 the binding energies as function of box size in terms of the substrate rather than on the metal atom.

color	m	r^2	B (eV nm ²)	$\Delta E(\infty)$ (eV)
red	8	0.788	-0.0367 ± 0.009	-1.502 ± 0.005
blue	7	0.878	-0.0721 ± 0.021	-1.495 ± 0.006
green	6	0.971	-0.1168 ± 0.043	-1.488 ± 0.008
brown	5	0.998	-0.1492 ± 0.082	-1.485 ± 0.013

Table S4: **Fittings for Al/(8,0) CNT.** Fitting parameters B and $\Delta E(\infty)$, as well as the coefficient of determination r^2 , for the curves in Fig. S2. The fitting parameters are reported within a standard error that we obtain by assuming uniform variance scale estimator and weights proportional to the DFT error of 0.01 eV.

color	m	r^2	B (eV nm ²)	$\Delta E(\infty)$ (eV)
red	8	0.903	0.143 ± 0.007	-1.300 ± 0.005
blue	7	0.935	-0.150 ± 0.013	-1.282 ± 0.007
green	6	0.996	-0.172 ± 0.024	-1.289 ± 0.009
brown	5	0.999	-0.181 ± 0.043	-1.291 ± 0.013

Table S5: **Fittings for Al/Graphene.** Fitting parameters B and $\Delta E(\infty)$, as well as the coefficient of determination r^2 , for the curves in Fig. S3. The fitting parameters are reported within a standard error that we obtain by assuming uniform variance scale estimator and weights proportional to the DFT error of 0.01 eV.

V. NUMERICAL CONVERGENCE

In this section, we provide further details of the numerical accuracy of the binding energies reported here from DFT calculations.

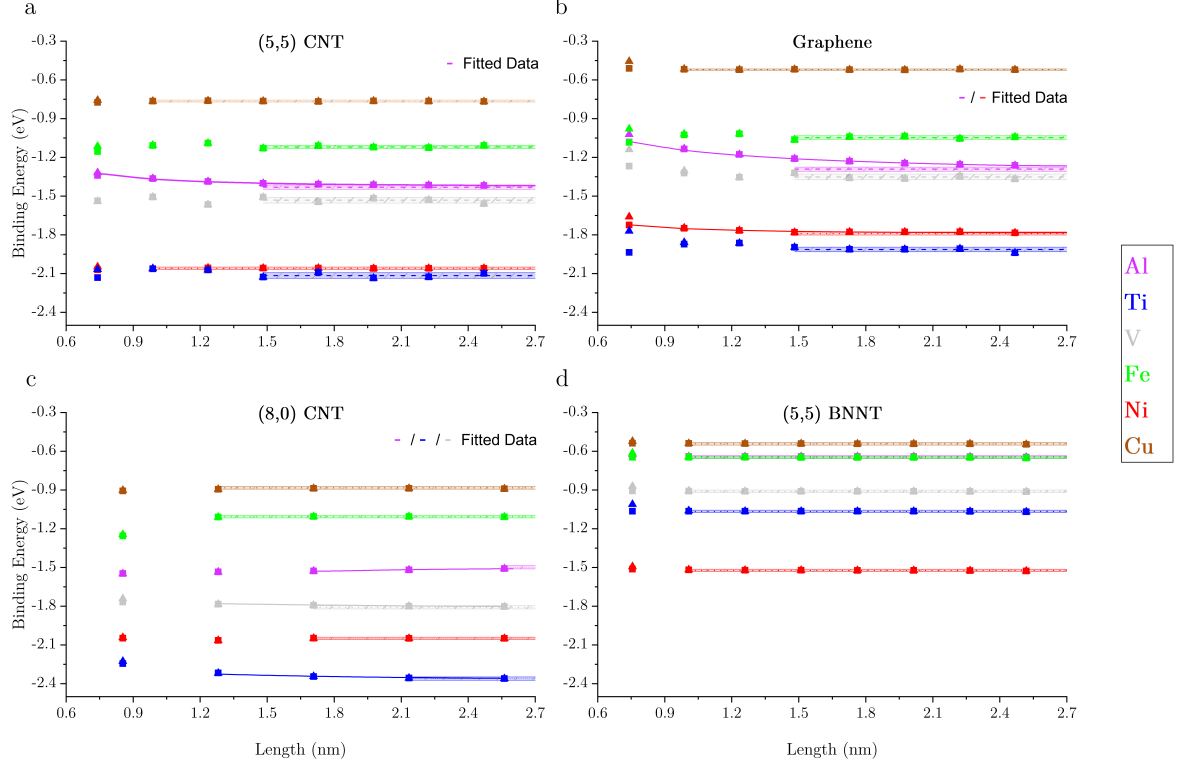


Figure S4: **Binding energies versus system size in a substrate-based comparison.** Here, the blue, red, grey, purple, green, and brown data points represent the add atoms Ti, Ni, V, Al, Fe and Cu, respectively. The squares show the results using the absolute ground state energy of the free atoms, whereas the triangles represent the results from the free atom in the respective adsorption size cells. A dotted line indicates fully converged DFT data, whereas dashed lines indicate the extrapolated binding energy (numerical fitting to Eq. 8 in case of Al for the (5,5) CNT and graphene) or averaged binding energy over the indicated data points (V, Fe, and Ti for graphene and the (5,5) CNT). In all cases, the shaded area represents the error in the binding energy originating from the DFT calculations. The solid line represents a fit to the scaling form in Eq. (8) from the TB model. Additional specifications are given in Fig. 2.

System	B (eV nm ²)	σ_B (eV nm ²)	$\Delta E(\infty)$ (eV)	$\sigma_{\Delta E(\infty)}$ (eV)
Al Graphene	-0.1807	0.0431	-1.291	0.013
Al (5,5) CNT	-0.0564	0.0431	-1.427	0.013
Al (8,0) CNT	-0.1492	0.0433	-1.485	0.008
Ti (8,0) CNT	-0.0730	0.024	-2.375	0.008
V (8,0) CNT	0.0405	0.0227	-1.808	0.007
Ni Graphene	0.0369	0.0068	-1.789	0.006

Table S6: **Fitting parameters for Fig. 2.** Fittings parameters B and $\Delta E(\infty)$, and their corresponding standard errors, σ_B and $\sigma_{\Delta E(\infty)}$, for the fitting curves reported in Fig. 2 in the main text.

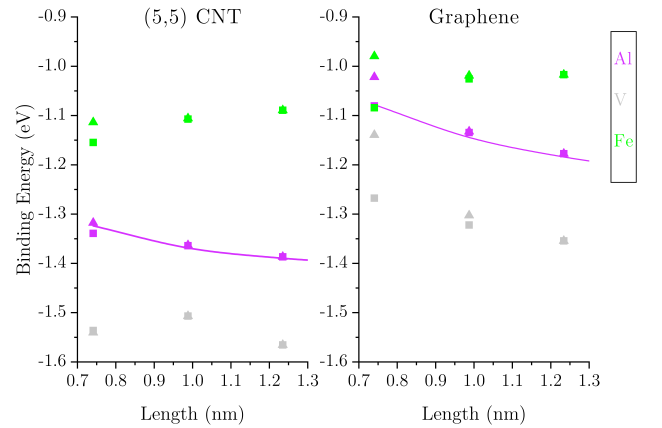


Figure S5: **Binding energies versus system size.** We show a close up of the variation in binding strength at shorter (5,5) CNTs (left) and smaller graphene sheets (right), for Al, V and Fe. The cell size varies from 0.7 nm to 1.3 nm.

3×3 supercell of Graphene						
$E_{\text{cut-off}}$ (eV)	Al	Ti	Cu	Fe	Ni	V
400	-1.062	-2.141	-0.484	-1.037	-1.700	-1.265
450	-1.064	-2.143	-0.486	-1.039	-1.701	-1.266
500	-1.064	-2.143	-0.486	-1.040	-1.702	-1.267
550	-1.064	-2.143	-0.487	-1.040	-1.702	-1.267
600	-1.065	-2.143	-0.487	-1.040	-1.702	-1.267
1×1×3 supercell of (5,5) BNNT						
$E_{\text{cut-off}}$ (eV)	Al	Ti	Cu	Fe	Ni	V
400	-0.623	-1.274	-0.523	-0.559	-1.492	-0.908
450	-0.623	-1.275	-0.522	-0.560	-1.492	-0.909
500	-0.624	-1.275	-0.523	-0.561	-1.493	-0.910
550	-0.622	-1.273	-0.521	-0.559	-1.490	-0.908
600	-0.622	-1.273	-0.521	-0.559	-1.491	-0.908

Table S7: **Convergence of the energy cut-off $E_{\text{cut-off}}$.** Convergence of $E_{\text{cut-off}}$ of Al, Ti, Cu, Fe, Ni and V adsorbing to a 3×3 supercell of graphene (top) and the 1×1×3 supercell of (5,5) BNNT (bottom). The convergence is tested through the binding strength of each metal atom to the substrate. Although an energy cut-off of 400 eV looks sufficient, due to the nature of our investigation we opted for an 450 eV cut-off.

k-mesh	Al	Ti	Cu	Fe	Ni	V
1×1×1	-1.672	-4.040	-0.939	-2.270	-2.323	-3.484
2×2×1	-0.671	-1.716	-0.483	-1.028	-1.698	-1.114
3×3×1	-1.077	-2.073	-0.611	-1.201	-1.770	-1.468
4×4×1	-1.071	-1.921	-0.493	-1.069	-1.731	-1.258
5×5×1	-1.075	-1.948	-0.556	-1.112	-1.731	-1.265
6×6×1	-1.045	-1.916	-0.500	-1.075	-1.726	-1.262
7×7×1	-1.074	-1.942	-0.532	-1.092	-1.724	-1.280
8×8×1	-1.084	-1.929	-0.507	-1.076	-1.721	-1.256
9×9×1	-1.068	-1.929	-0.515	-1.086	-1.723	-1.264
10×10×1	-1.069	-1.924	-0.509	-1.077	-1.720	-1.261
11×11×1	-1.080	-1.932	-0.510	-1.082	-1.723	-1.263
12×12×1	-1.080	-1.926	-0.509	-1.077	-1.719	-1.258
13×13×1	-1.075	-1.928	-0.510	-1.080	-1.722	-1.263
14×14×1	-1.075	-1.926	-0.509	-1.077	-1.719	-1.260
15×15×1	-1.078	-1.928	-0.510	-1.079	-1.721	-1.260

Table S8: **Monkhorst Pack mesh convergence test in graphene.** The test is performed for Al, Ti, Cu, Fe, Ni and V on the 3×3 supercell of graphene. Convergence is tested through the binding strength of each metal atom to the substrate, reported in eV. As a result, we conclude that for this substrate, a k -point mesh of 11×11×1 is required to obtain converged results in the binding energies in all cases.

k-mesh	Al	Ti	Cu	Fe	Ni	V
1×1×1	-0.806	-2.080	-0.709	-0.993	-2.09	-1.432
1×1×2	-1.524	-2.464	-0.823	-1.204	-2.19	-1.772
1×1×3	-1.305	-2.201	-0.668	-0.970	-1.96	-1.516
1×1×4	-1.185	-2.171	-0.695	-0.995	-2.03	-1.442
1×1×5	-1.266	-2.231	-0.724	-1.032	-2.04	-1.434
1×1×6	-1.370	-2.329	-0.772	-1.107	-2.07	-1.545
1×1×7	-1.348	-2.289	-0.757	-1.082	-2.02	-1.521
1×1×8	-1.329	-2.240	-0.720	-1.035	-2.01	-1.473
1×1×9	-1.332	-2.253	-0.731	-1.044	-2.03	-1.484
1×1×10	-1.343	-2.271	-0.752	-1.068	-2.04	-1.502
1×1×11	-1.345	-2.271	-0.751	-1.069	-2.04	-1.501
1×1×12	-1.339	-2.266	-0.745	-1.062	-2.03	-1.496
1×1×13	-1.338	-2.265	-0.744	-1.061	-2.03	-1.496
1×1×14	-1.339	-2.266	-0.745	-1.062	-2.04	-1.497
1×1×15	-1.339	-2.266	-0.745	-1.062	-2.03	-1.497

Table S9: **Monkhorst Pack mesh convergence test in (5,5) CNT.** The test is performed for Al, Ti, Cu, Fe, Ni and V on the 1×1×4 supercell of (5,5) CNT. Convergence is tested through the binding strength of each metal atom to the substrate, reported in eV. As a result, we conclude that for this substrate, a k -point mesh of 1×1×10 is required to obtain converged results in the binding energies in all cases.

k-mesh	Al	Ti	Cu	Fe	Ni	V
1×1×1	-1.858	-3.299	-1.161	-1.612	-2.247	-2.428
1×1×2	-1.282	-2.406	-0.794	-1.175	-2.045	-1.727
1×1×3	-1.541	-2.457	-0.913	-1.221	-2.051	-1.769
1×1×4	-1.553	-2.448	-0.854	-1.213	-2.058	-1.716
1×1×5	-1.505	-2.453	-0.889	-1.215	-2.055	-1.750
1×1×6	-1.506	-2.447	-0.878	-1.214	-2.056	-1.740
1×1×7	-1.528	-2.453	-0.881	-1.214	-2.055	-1.754
1×1×8	-1.532	-2.449	-0.883	-1.214	-2.056	-1.763
1×1×9	-1.518	-2.453	-0.878	-1.215	-2.056	-1.764
1×1×10	-1.517	-2.450	-0.883	-1.215	-2.056	-1.763
1×1×11	-1.528	-2.453	-0.881	-1.215	-2.056	-1.763
1×1×12	-1.529	-2.451	-0.881	-1.215	-2.056	-1.764
1×1×13	-1.522	-2.453	-0.882	-1.215	-2.056	-1.764
1×1×14	-1.522	-2.452	-0.880	-1.215	-2.056	-1.763
1×1×15	-1.528	-2.453	-0.883	-1.215	-2.056	-1.764

Table S10: **Monkhorst Pack mesh convergence test in (8,0) CNT.** The test is performed for Al, Ti, Cu, Fe, Ni and V on the 1×1×3 supercell of (8,0) CNT. Convergence is tested through the binding strength of each metal atom to the substrate, reported in eV. As a result, we conclude that for this substrate, a k -point mesh of 1×1×5 is required to obtain converged results in the binding energies in the cases of Ti, Cu, Fe, and Ni; a k -point mesh of 1×1×7 in the case of Al, and 1×1×8 for V.

k-mesh	Al	Ti	Cu	Fe	Ni	V
1×1×1	-0.635	-1.273	-0.540	-0.564	-1.509	-0.924
1×1×2	-0.623	-1.274	-0.522	-0.560	-1.491	-0.904
1×1×3	-0.623	-1.273	-0.522	-0.559	-1.492	-0.903
1×1×4	-0.623	-1.273	-0.522	-0.559	-1.492	-0.903
1×1×5	-0.623	-1.273	-0.522	-0.559	-1.492	-0.903
1×1×6	-0.623	-1.273	-0.522	-0.559	-1.492	-0.903

Table S11: **Monkhorst Pack mesh convergence test in (5,5) BNNT.** The test is performed for Al, Ti, Cu, Fe, Ni and V on the 1×1×3 supercell of (5,5) BNNT. Convergence is tested through the binding strength of each metal atom to the substrate, reported in eV. As a result, we conclude that for this substrate, a k -point mesh of 1×1×2 is required to obtain converged results in the binding energies in all cases.

System	1 nm (eV)	2 nm (eV)	Energy Difference (eV)
clean surface	-297.446	-297.424	-0.022
Fe	-300.796	-301.168	-0.372
Fe (fixed)	-301.746	-301.709	-0.037
Ni	-299.722	-299.691	-0.031
Al	-297.972	-297.940	-0.033
Cu	-298.168	-298.122	-0.046
Ti	-301.334	-301.291	-0.043

Table S12: **Layer spacing test using the 4×4 Graphene supercell.** The total energies of Al, Ti, Fe, Ni, and Cu are presented for a 1 nm and 2 nm layer spacing. Note that in the case of Fe, the T site (fixed) is tested next to the H site since it presents a local minimum, with the H site being the preferred adsorption site. The term “fixed” in the case of Fe indicates that Fe was constrained at this position. All other adsorption cases took place at the H site.

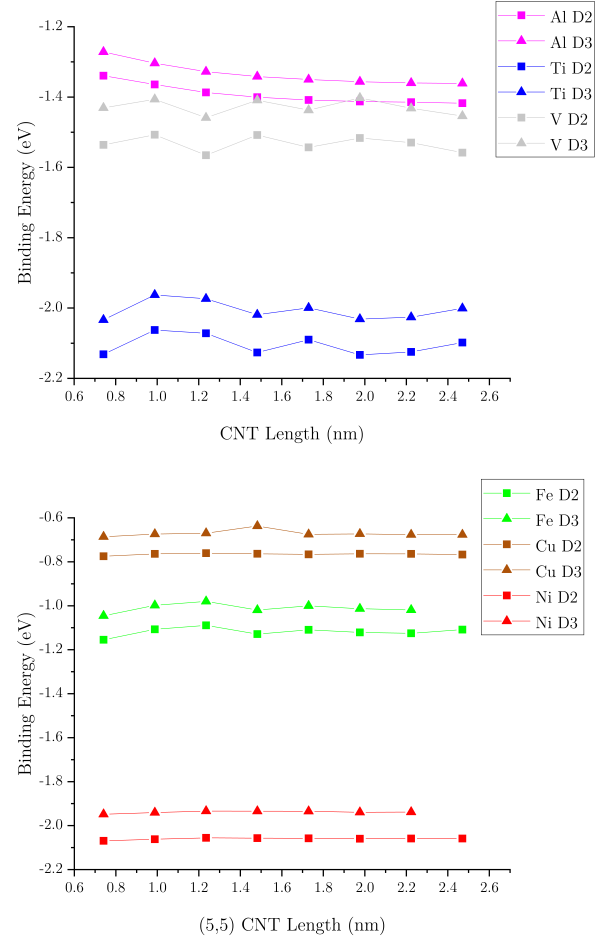


Figure S6: **Binding energies obtained from two different dispersion correction methods.** Binding energies D2 versus D3 (Grimme) of Al, Ti and V (top) and Fe, Ni and Cu (bottom) adsorbing to the (5,5) CNT of different length.